Anisotropic magneto-optical effects in $CdTe/Cd_{0.75}Mn_{0.25}Te$ quantum wire structures

Yukihiro Harada, Takashi Kita,* and Osamu Wada
Department of Electrical and Electronics Engineering, Graduate School of Engineering, Kobe University, Rokkodai 1-1, Nada, Kobe 657-8501, Japan

Hiroaki Ando
Department of Physics, Faculty of Science and Engineering, Konan University, Okamoto 8-9-1, Higashi-Nada, Kobe 658-8501, Japan

Henri Mariette
Laboratoire de Spectrométrie Physique, Université J. Fourier, Grenoble I, CNRS (UMR 5588), Boîte Postale 87, F-38402 Saint Martin d'Hères, Cedex, France

(Received 18 February 2008; revised manuscript received 15 June 2008; published 20 August 2008)

Anisotropic magneto-optical effects in CdTe/CdMnTe quantum wire structures have been studied theoretically by using the multiband effective-mass method. The Mn spatial distribution influences not only the lateral quantum confinement of the carrier wave function but also the exchange coupling of spins between the carrier and Mn ions. The anisotropic configuration between the spin of holes confined in the wire and the Mn spin oriented by the magnetic field causes anisotropy in the magnetic-field dependence of the valence-band structure, and this results in the anisotropic Zeeman shift and linear polarization properties of the optical transition depending on the spin configuration.

DOI: 10.1103/PhysRevB.78.073304 PACS number(s): 78.67.Lt, 75.50.Pp, 75.75.+a, 78.20.Ls

I. INTRODUCTION

Control of carrier spins in semiconductor heterostructures and nanostructures has attracted considerable interest in this decade for the realization of spin electronics and quantum information processing devices.[1–3] Diluted magnetic semiconductors (DMSs) are promising materials leading to substantial spin-related phenomena, such as Faraday rotation, Zeeman shift, and exciton magnetic polaron (EMP) formation, which are caused by the *s-d* (*p-d*) spin-exchange interaction between electrons (holes) and magnetic ions.[4] In the low-dimensional DMS heterostructures, the exchange interaction between the confined carriers and magnetic spins induces anisotropic magneto-optical properties depending on the external magnetic-field directions. For example, the hole spin in the DMS quantum wells is reoriented in a strong field in the Voigt configuration by the *p-d* exchange interaction, and thereby the valence-band mixing is induced.[5–7] On the other hand, recently, the exchange interaction between a single exciton and a single magnetic atom in a Mn-doped quantum dot has been demonstrated to show dramatic fan diagrams in the Faraday and Voigt configurations.[8] In contrast to these heavy-hole-dominant confined cases, excitons in a quantum wire (QWR) are significantly affected by the light-hole components.[9–11] Since the light-hole component has finite in-plane *g* factor, dramatic changes are expected to appear in the magneto-optical properties of the DMS QWRs even under weak magnetic field applied in the Voigt configuration.[12–14]

We have recently demonstrated remarkable anisotropic Zeeman shifts and hole-spin reorientation in $CdTe/Cd_{0.75}Mn_{0.25}Te$ tilted superlattices (TSLs) in the Voigt configuration.[15,16] This TSL structure consists of QWRs of CdTe sandwiched by CdMnTe barriers. A large Zeeman shift of about 30 meV in 5 T suggests a modulation of the Mn composition in the QWRs caused by interdiffusion between Cd and Mn atoms.[17] The spatial distribution of Mn composition influences both the lateral quantum confinement and the *sp-d* exchange coupling. Since the interface structure between the magnetic and nonmagnetic regions affects the exchange interaction,[18–20] the anisotropic magneto-optical properties found in the $CdTe/Cd_{0.75}Mn_{0.25}Te$ QWRs are considered to be characterized by the spatial distribution of Mn composition. In this Brief Report, we have theoretically studied the anisotropic behavior of the Zeeman shift and the optical polarization properties of the $CdTe/Cd_{0.75}Mn_{0.25}Te$ QWRs in the Voigt configuration by using the multiband effective-mass method.

II. CALCULATIONS MODEL AND METHODS

In this section, we describe a theoretical analysis model and method for $CdTe/Cd_{0.75}Mn_{0.25}Te$ QWRs structure fabricated by the fractional monolayer growth. Here, we used a model of a Mn-composition modulation varying sinusoidally in the *x* direction as shown in Fig. 1. The continuous potential profile along the *x* direction as a function of the Mn composition is necessary for considering effects of the atomic interdiffusion of Mn. The spatial distribution of Mn composition x_{Mn} is given by

$$x_{Mn}(x) = Mn_{ave} - \Delta Mn \cos[(2\pi/L_x)x], \quad (1)$$

where Mn_{ave} and ΔMn are the average and modulation amplitude of Mn composition, respectively. L_x is the period of

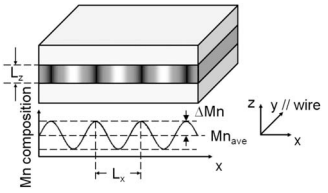

FIG. 1. $CdTe/Cd_{0.75}Mn_{0.25}Te$ QWRs structure fabricated by the fractional monolayer growth. The spatial distribution of Mn composition in the QWR plane is assumed to be sinusoidally modulated.

the spatial distribution of Mn composition and L_z corresponds to the thickness of the QWR layer sandwiched by infinitely high barriers. Treating the effect of the *sp-d* exchange interaction, we assumed that the Landau quantization effect is negligible compared to the huge Zeeman splitting. We have treated the *sp-d* exchange interaction by adding the Heisenberg-type Hamiltonian[21]

$$H_{s\text{-}d} = N_0 \alpha x_{\mathrm{Mn}} \langle \boldsymbol{S} \rangle \cdot \boldsymbol{s}, \tag{2}$$

$$H_{p\text{-}d} = (1/3) N_0 \beta x_{\mathrm{Mn}} \langle \boldsymbol{S} \rangle \cdot \boldsymbol{J}, \tag{3}$$

where $N_0\alpha$ ($N_0\beta$) is the *s-d* (*p-d*) exchange constant of $Cd_{1-x}Mn_xTe$, $\langle \boldsymbol{S} \rangle$ is the average component of the Mn spin along the magnetic-field direction, $\boldsymbol{s}$ is the electron-spin operator, and $\boldsymbol{J}$ is the hole total angular momentum operator. The exchange constant used is 0.22 (−0.88)eV for $N_0\alpha$ ($N_0\beta$).[21] The average component of the Mn spin is expressed by a modified Brillouin function B_S,[21]

$$\langle \boldsymbol{S} \rangle = S_0 B_{5/2}[Sg\mu_B |\boldsymbol{B}| / k_B (T + T_0)], \tag{4}$$

where $S=5/2$, $g=2$ for Mn. μ_B is the Bohr magneton, $|\boldsymbol{B}|$ is the absolute value of the applied magnetic field, and S_0 and T_0 are fitting parameters for the antiferromagnetic Mn-Mn coupling, respectively. Here, we assumed that the fitting parameters are related to the Mn composition by the following empirical expressions: $S_0(x_{\mathrm{Mn}}) = S[0.2635 \exp(-43.34 x_{\mathrm{Mn}}) + 0.729 \exp(-6.190 x_{\mathrm{Mn}}) + 0.00721]$ and $T_0(x_{\mathrm{Mn}}) = 35.37 x_{\mathrm{Mn}} / (1 + 2.752 x_{\mathrm{Mn}})$.[22] The *sp-d* exchange interaction exhibits a spatial distribution according to the Mn distribution. It is noted that the spatial distribution of the *sp-d* exchange energy also depends on the strength of the external magnetic field.

We assumed that the conduction and valence bands are decoupled, and, furthermore, effects of the spin-orbit split-off band are neglected because the spin-orbit split-off energy (0.9 eV) of CdTe is considerably larger than the intervalence-subband energy of several tens of meV. Therefore, we focus on the heavy- and light-hole mixing in the valence subbands near the band edge. The valence-band mixing induced by the one-dimensional quantum confinement is treated by using the multiband effective-mass method based on the four-band Luttinger-Kohn Hamiltonian H_{LK}.[23] A simple effective-mass model is used to describe the electron states in the conduction band.

The hole wave functions are represented by the expanded orthogonal function set,[24]

$$\psi_k^q(\boldsymbol{r}) = (1/\sqrt{L_x L_z}) \sum_{mnj} C_{jk}^{qmn} \exp(-imKx) \times \sin[(n\pi/L_z)z] \exp(-ik_x x - ik_y y) u_j^v,$$

$$K = 2\pi/L_x, \quad -\pi/L_x \le k_x \le \pi/L_x, \tag{5}$$

where m and n are the indices of the hole envelope functions in the x and z directions, respectively. C_{jk}^{qmn} is the expansion coefficient, u_j is the Bloch function at the top of valence band, and q is the index of the valence subbands from the highest subband. Substituting the expanded wave function into the matrix equation,

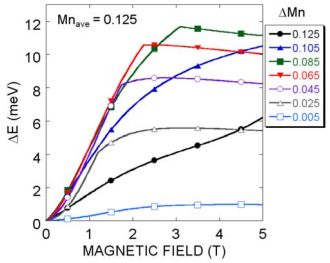

FIG. 2. (Color online) Magnetic-field dependence of the Zeeman shift anisotropy for various ΔMn at Mn_{ave} of 0.125. The Zeeman shift anisotropy is defined by the $\Delta E = E_{B\perp \mathrm{wire}}^{\mathrm{Zeeman}} - E_{B\parallel \mathrm{wire}}^{\mathrm{Zeeman}}$, where $E_{B\perp \mathrm{wire}}^{\mathrm{Zeeman}}$ and $E_{B\parallel \mathrm{wire}}^{\mathrm{Zeeman}}$ are the Zeeman shift energy in the magnetic field applied perpendicular and parallel to the QWR direction, respectively.

$$[H_{\mathrm{LK}} + V_h(x,z) + H_{p\text{-}d} - E_k^{vq}] \psi_k^q(\boldsymbol{r}) = 0, \tag{6}$$

we get a secular equation to be solved for the eigenenergies E_k^{vq} and the eigenvectors C_{jk}^{qmn} of each valence subband. $V_h(x,z)$ indicates the spatial distribution of the potential for the hole. The wave function distribution of the envelope components at the Γ point in the qth valence subbands can be expanded using the eigenvectors C_j^{qmn} by $\Sigma_{u_j} |\langle u_j^v | \psi^q(\boldsymbol{r}) \rangle|^2$. By using a similar method for the electron wave functions, we obtain the eigenenergies E_k^{cp} and the eigenvectors $D_{\sigma k}^{pmn}$ of each conduction subband, where p is the index of the conduction subbands from the lowest subband. The anisotropy of the optical transition probability at the Γ point is expressed as[24]

$$K_{pq} = (1/2)(|J_{3/2}^{pq}|^2 + |J_{-3/2}^{pq}|^2) + (1/6)(|J_{1/2}^{pq}|^2 + |J_{-1/2}^{pq}|^2) \pm (1/2\sqrt{3})(J_{3/2}^{*pq} J_{-1/2}^{pq} + J_{1/2}^{*pq} J_{-3/2}^{pq} + \mathrm{c.c.}),$$

$$J_j^{pq} = \sum_{mn\sigma} D_\sigma^{pmn*} C_j^{qmn} \delta_{\sigma \pm 1, j}. \tag{7}$$

The plus and minus in the third term in Eq. (7) correspond to the parallel and perpendicular polarization component to the QWR, respectively. In this study, we neglect effects of the electron-hole Coulomb interaction because the linear polarization characteristics of the oscillator strength is insensitive to the electron-hole Coulomb interaction in the QWRs.[10] Based on our experimental sample structure,[15] L_x and L_z are 20 nm and 10 nm, respectively. In our calculations, we used the Luttinger parameters $\gamma_1 = 5.38$, $\gamma_2 = \gamma_3 = 1.89$,[25] and the valence-band offset $Q_v = 0.30$.[26]

III. NUMERICAL RESULTS AND DISCUSSIONS

Figure 2 shows calculated typical magnetic-field dependences of the Zeeman shift anisotropy for various ΔMn at Mn_{ave} of 0.125. The Zeeman shift anisotropy is defined by the $\Delta E = E_{B\perp \mathrm{wire}}^{\mathrm{Zeeman}} - E_{B\parallel \mathrm{wire}}^{\mathrm{Zeeman}}$, where $E_{B\perp \mathrm{wire}}^{\mathrm{Zeeman}}$ and $E_{B\parallel \mathrm{wire}}^{\mathrm{Zeeman}}$ are the Zeeman shift energy in the magnetic field applied perpendicular and parallel to the QWR direction, respectively. Such anisotropy results from the anisotropic field dependence of the Zeeman diagram of the valence bands. Figures 3(a) and 3(b) display the Zeeman diagrams of the valence subbands near the band edge in the ΔMn=0.020 in the perpendicular and parallel magnetic field, respectively. The Zeeman dia-

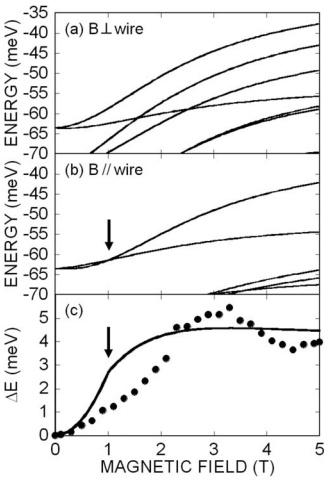

FIG. 3. The Zeeman diagrams of the valence subbands near the band edge in the (a) perpendicular and (b) parallel magnetic field, respectively, for $\Delta Mn=0.020$ and $Mn_{ave}=0.125$. (c) Measured (closed circle) and calculated (solid line) Zeeman shift anisotropy as a function of the magnetic field.

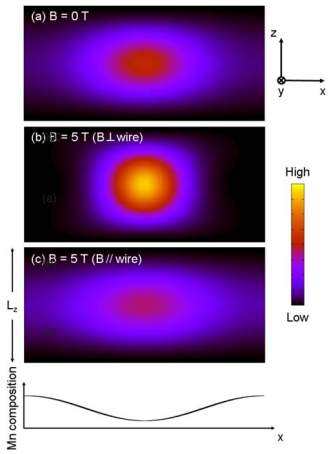

FIG. 4. (Color online) Cross-sectional images of the envelope components of the highest valence-subband wave function in the QWR for $\Delta Mn=0.020$ and $Mn_{ave}=0.125$. The cross-sectional area is $L_x/L_z=20$ nm/10 nm. (a), (b), and (c) are results in the zero magnetic field, the perpendicular magnetic field, and the parallel magnetic field, respectively.

gram shows significant anisotropy depending on the applied field direction. The Zeeman shift in the parallel magnetic field is suppressed in contrast to that in the perpendicular magnetic field. When $\Delta Mn=0.005$, the Zeeman shift anisotropy is small as shown in Fig. 2 because of the weak lateral quantum confinement. When ΔMn increases ($0.025 \leq \Delta Mn \leq 0.085$), the Zeeman shift anisotropy becomes larger owing to the stronger lateral quantum confinement. However, when ΔMn increases further ($0.105 \leq \Delta Mn \leq 0.125$), the Zeeman shift anisotropy becomes small again because the much stronger confinement leads to the reduction of spatial overlapping between the hole wave function and Mn spins. Furthermore, it is noted that the Zeeman shift anisotropy shows saturation for ΔMn below 0.085. That saturation originates from the hole-spin reorientation in the parallel magnetic field, which induces the decrease in the valence-band states anisotropy. The hole-spin reorientation is represented by an intersection of the highest valence subband as indicated by an arrow in Fig. 3(b). The magnetic field representing the hole-spin reorientation depends on ΔMn. For example, for smaller ΔMn, a weak magnetic field is enough to rotate the hole spin to the external field because of the weaker lateral quantum confinement.

Figure 3(c) compares measured (closed circle) and calculated (solid line) anisotropic Zeeman shifts as a function of the magnetic field. Magneto-photoluminescence (PL) for the same sample structure has been carried out at 1.5 K. Detailed sample structure and experimental results have been reported in Ref. 15. The measured anisotropy tends to saturate above 3 T,[15] which can be reproduced in our calculation. Here, the calculated potential barrier along the x direction in the valence band is about 19 meV when ΔMn is 0.020. That barrier confines the highest valence-subband state focused here. On the other hand, the potential barrier for the hole along the z direction is estimated to be 66 meV,[15] which is about three times larger than that along the x direction. We believe, therefore, our assumption about the infinite wall along the z direction safely explains the experimental results. Obviously, the saturation is caused by the valence-band crossing as shown in Fig. 3(b). Therefore, the anisotropic Zeeman effects in the $CdTe/Cd_{0.75}Mn_{0.25}Te$ QWRs are concluded to be characterized by the hole-spin reorientation in the parallel magnetic field. The slight discrepancy observed in the weak magnetic fields less than 2 T would be caused by the EMP formation, which was neglected in our calculation.

Figure 4 displays cross-sectional images of the envelope components of the highest valence-subband wave function. Figures 4(a)–4(c) are results in the zero magnetic field, the perpendicular magnetic field, and the parallel magnetic field, respectively. Here, the magnitude of the applied magnetic field is 5 T. As shown in Fig. 4(a), the envelope component of the highest valence-subband wave function is highly peaked near the wire structure along the x direction. The electron and hole wave functions are localized in the two directions, and, therefore, delocalized along one direction (y direction), induces the one-dimensional characters. In the perpendicular magnetic field [Fig. 4(b)], the wave function is compressed along the x direction as compared to that in the zero magnetic field, whereas the wave function in the parallel magnetic field [Fig. 4(c)] is extended. These results indicate that the quantization along the x direction is strengthened in the perpendicular magnetic field. On the other hand, in the parallel magnetic field, the hole-spin reorientation to the external field direction reduces the quantization along the x direction and generates new quantization along the y direction. These anisotropic magnetic-field dependences of the wave function do not appear in ideal CdMnTe QWRs surrounded by an infinite barrier,[13] and so they are characteristic features of the composition modulated structure in the real CdTe/CdMnTe QWRs.

Next, we discuss linear optical polarization properties in the magnetic field. Figure 5(a) shows the field dependence of the linear polarization of the measured magneto-PL.[16] The linear polarization is defined by $P=(I_{\parallel}-I_{\perp})/(I_{\parallel}+I_{\perp})$, where $I_{\parallel}$ and $I_{\perp}$ are parallel and perpendicular polarization components of the PL intensity to the QWR direction, respectively.

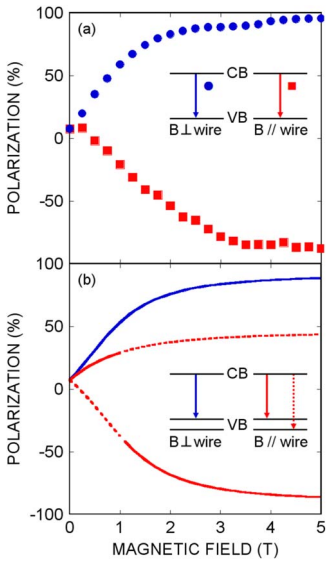

FIG. 5. (Color online) Magnetic-field dependence of the linear polarization of (a) measured magneto-PL and (b) calculated optical transition probability for $\Delta Mn=0.020$ and $Mn_{ave}=0.125$. Blue and red lines indicate results for perpendicular and parallel magnetic field, respectively. Solid and dashed lines are polarizations for transitions to the highest and second highest valence subbands, respectively.

Here we adjusted the zero-field optical polarization to a theoretically calculated value mentioned below. When applying the perpendicular magnetic field, the measured parallel polarization component $I_{\parallel}$ was observed to increase as plotted by closed circles in Fig. 5(a) because the quantization along the x direction is strengthened as shown in Fig. 4(b). On the other hand, in the parallel magnetic field, the polarization changes from a positive value to a negative one. Finally, the perpendicular polarization component $I_{\perp}$ becomes dominant in the high magnetic field as a result of the quantization along the y direction caused by the hole-spin reorientation. Such asymmetric behavior depending on the applied field direction is noted to be a characteristic feature of the QWR. Calculated field dependences of the linear polarization feature corresponding to these experimental results are summarized in Fig. 5(b). Blue and red lines indicate the results for perpendicular and parallel magnetic fields, respectively. Solid and dashed lines are polarizations for transitions to the highest and second highest valence subbands, respectively. The calculation has been performed for $\Delta Mn=0.020$ and $Mn_{ave}=0.125$. The calculated zero-field optical polarization is 7%. In the perpendicular magnetic field, the calculated linear polarization properties reproduce well the measured results. On the other hand, in the parallel magnetic field, the calculated polarization of the optical transition to the highest valence subband shows an abrupt jump at about 1 T, where the valence-band crossing occurs as shown in Fig. 3(b). Such abrupt change cannot be confirmed in the experimental result indicated by the square symbols in Fig. 5(a). To understand the discrepancy, we need to consider the inhomogeneous broadening of the PL spectrum. The broadening of the measured PL spectrum amounts to ~20 meV,[15] which is over the splitting energy shown in Fig. 3(b). In particular for the low magnetic fields less than 3 T, both the split transitions near the edge must be considered. Therefore, the polarizations in these fields are considered to show almost intermediate values. Such consideration explains the continuous, monotonic change of the experimental results.

IV. CONCLUSIONS

In summary, we have studied the anisotropic magneto-optical effects in CdTe/CdMnTe QWRs by using the multiband effective-mass method. The Mn spatial distribution influences not only the lateral quantum confinement of the carrier wave function but also the exchange coupling of spins between the carrier and Mn ions. The calculated anisotropic Zeeman shift and linear polarization properties of the optical transition agree well with the experimental results. The anisotropic configuration between the hole spin and the Mn spin oriented by the external magnetic field is a key factor to control the anisotropy in the magnetic-field dependence of the valence-band structure.

ACKNOWLEDGMENTS

This work was partially supported by the Japan Society for the Promotion of Science.

*kita@eedept.kobe-u.ac.jp

[1] S. A. Wolf *et al.*, Science **294**, 1488 (2001).
[2] *Semiconductor Spintronics and Quantum Computation*, edited by D. D. Awschalom, D. Loss, and N. Samarth (Springer-Verlag, Heidelberg, 2002).
[3] I. Zutić *et al.*, Rev. Mod. Phys. **76**, 323 (2004).
[4] J. K. Furdyna, J. Appl. Phys. **64**, R29 (1988).
[5] P. Peyla *et al.*, Phys. Rev. B **47**, 3783 (1993).
[6] B. Kuhn-Heinrich *et al.*, Solid State Commun. **91**, 413 (1994).
[7] D. Suisky *et al.*, Phys. Rev. B **58**, 3969 (1998).
[8] Y. Léger *et al.*, Phys. Rev. B **72**, 241309(R) (2005).
[9] U. Bockelmann and G. Bastard, Phys. Rev. B **45**, 1688 (1992).
[10] H. Ando *et al.*, Phys. Rev. B **55**, 2429 (1997).
[11] F. Vouilloz *et al.*, Phys. Rev. Lett. **78**, 1580 (1997).
[12] F. V. Kyrychenko and J. Kossut, Phys. Rev. B **61**, 4449 (2000).
[13] Y. Harada *et al.*, Phys. Rev. B **74**, 245323 (2006).
[14] X.-W. Zhang *et al.*, Phys. Rev. B **76**, 195306 (2007).
[15] S. Nagahara *et al.*, Phys. Rev. B **69**, 233308 (2004).
[16] T. Kita *et al.*, J. Cryst. Growth **275**, e2221 (2005).
[17] H. Mariette *et al.*, Microelectron. J. **30**, 329 (1999).
[18] J. M. Fatah *et al.*, Phys. Rev. B **49**, 10341 (1994).
[19] J. A. Gaj *et al.*, Phys. Rev. B **50**, 5512 (1994).
[20] A. Kudelski *et al.*, Phys. Rev. B **64**, 045312 (2001).
[21] J. A. Gaj *et al.*, Solid State Commun. **29**, 435 (1979).
[22] P. Kossacki *et al.*, Phys. Rev. B **70**, 195337 (2004).
[23] J. M. Luttinger, Phys. Rev. **102**, 1030 (1956).
[24] H. Ando *et al.*, J. Appl. Phys. **77**, 3372 (1995).
[25] T. Z. Kachlishvili, Solid State Commun. **80**, 283 (1991).
[26] B. Kuhn-Heinrich *et al.*, J. Appl. Phys. **75**, 8046 (1994).